Epitaxial Growth Modes

Phänomenologische Theorie
der Kristallabscheidung an Oberflächen. I

Von Ernst Bauer*

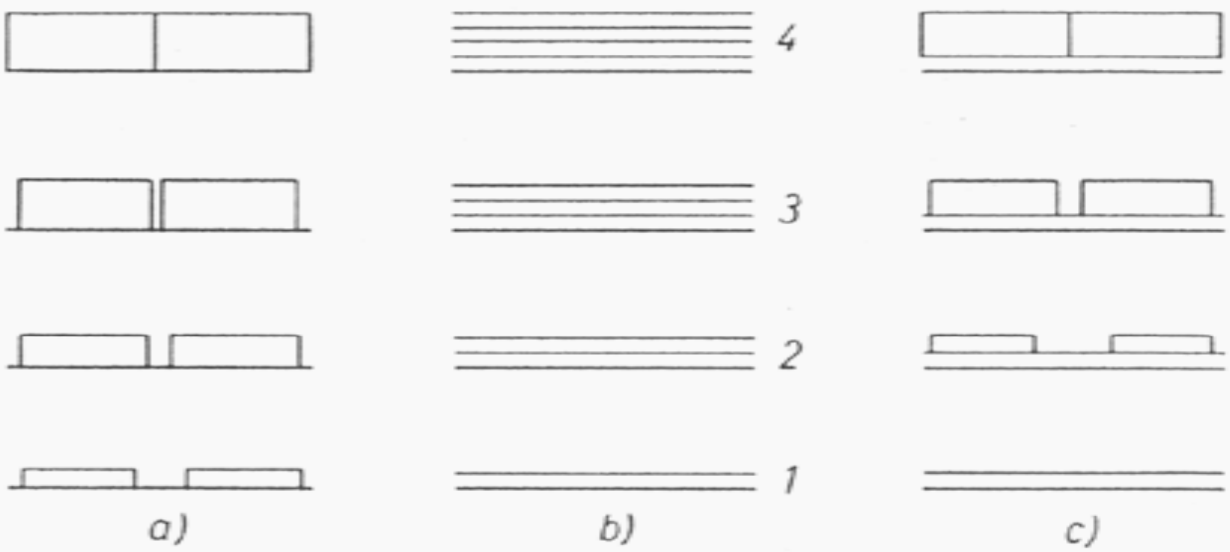

Abb. 3. Die verschiedenen Wachstumsmechanismen:
a) Volmer-Weber-Mechanismus, b) Frank-van-der-Merwe-Mechanismus,
c) Stranski-Krastanov-Mechanismus

Fig. 6.7

Dependence of Gibbs Free Energy on the Extent of Crystalline Phase

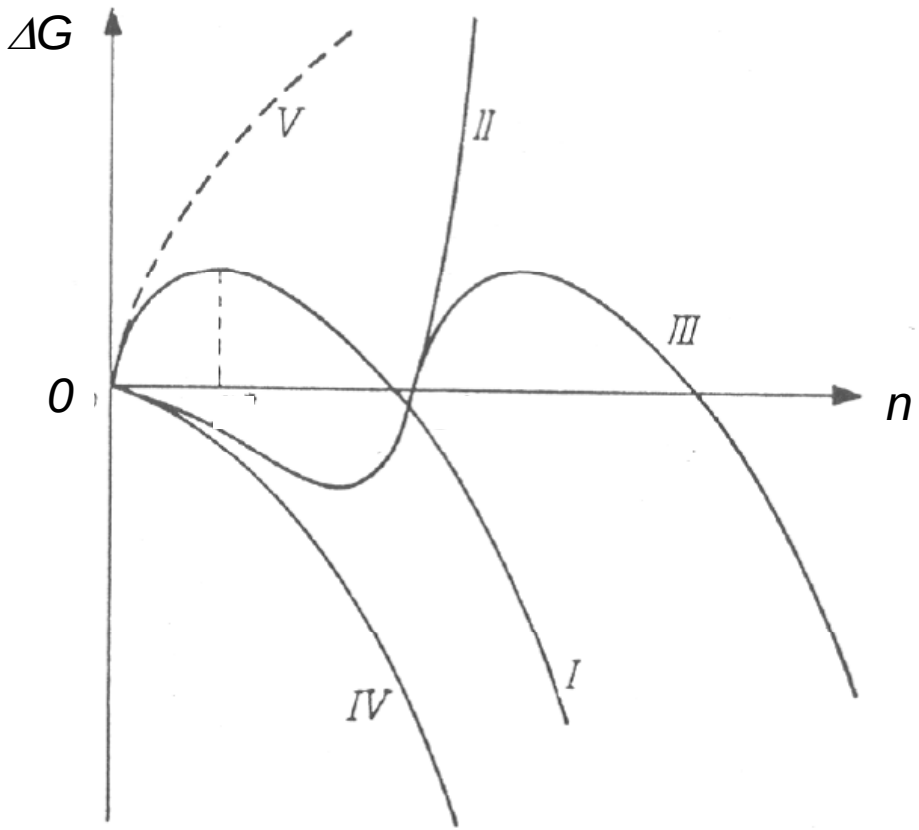

Abb. 1. *Change of Gibb`s free energy ΔG with particle number n in the crystalline phase*

Fig. 6.8

Vollmer – Weber Growth: Au Deposited on Defective Graphite

STM

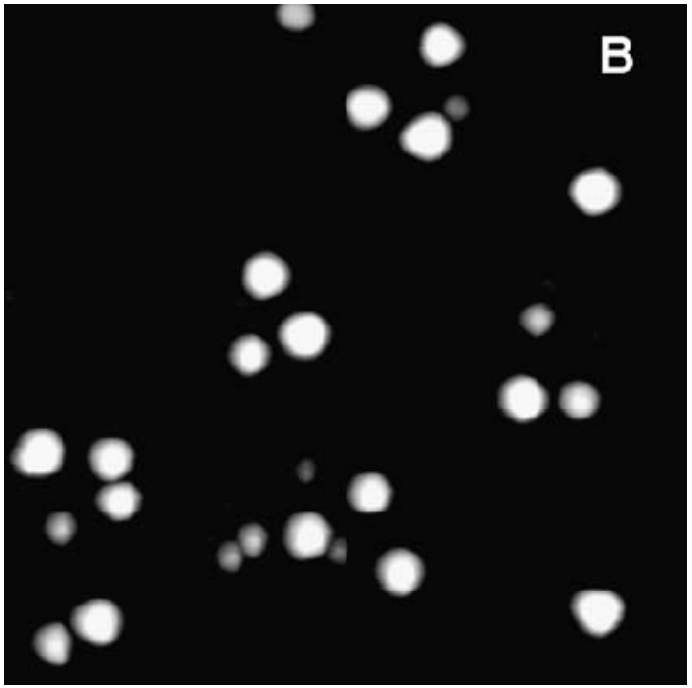

1000 Å

TEM

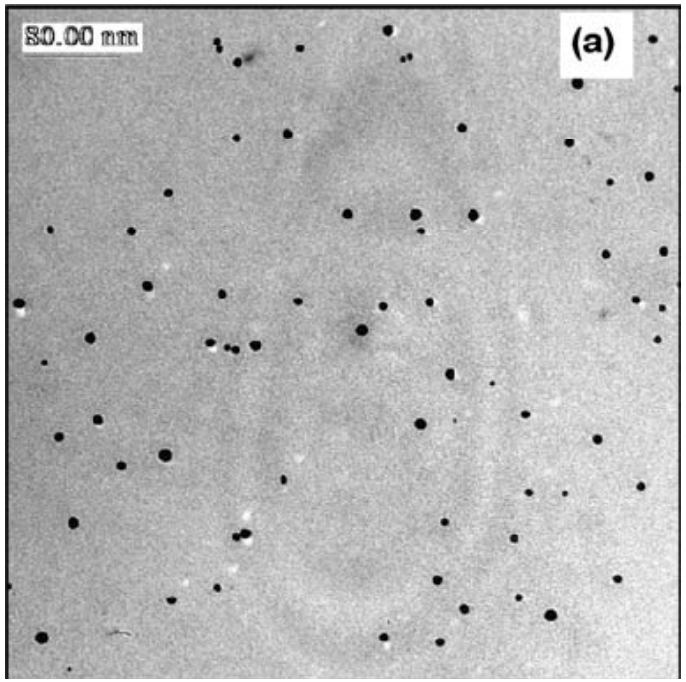

H. Hövel, I. Barke, Prog. in Surf. Sci. 81 (2006) 53

Fig. 6.9

Frank – van der Merwe Growth: Homoepitaxy of Pt on Pt(111)

8100 Å

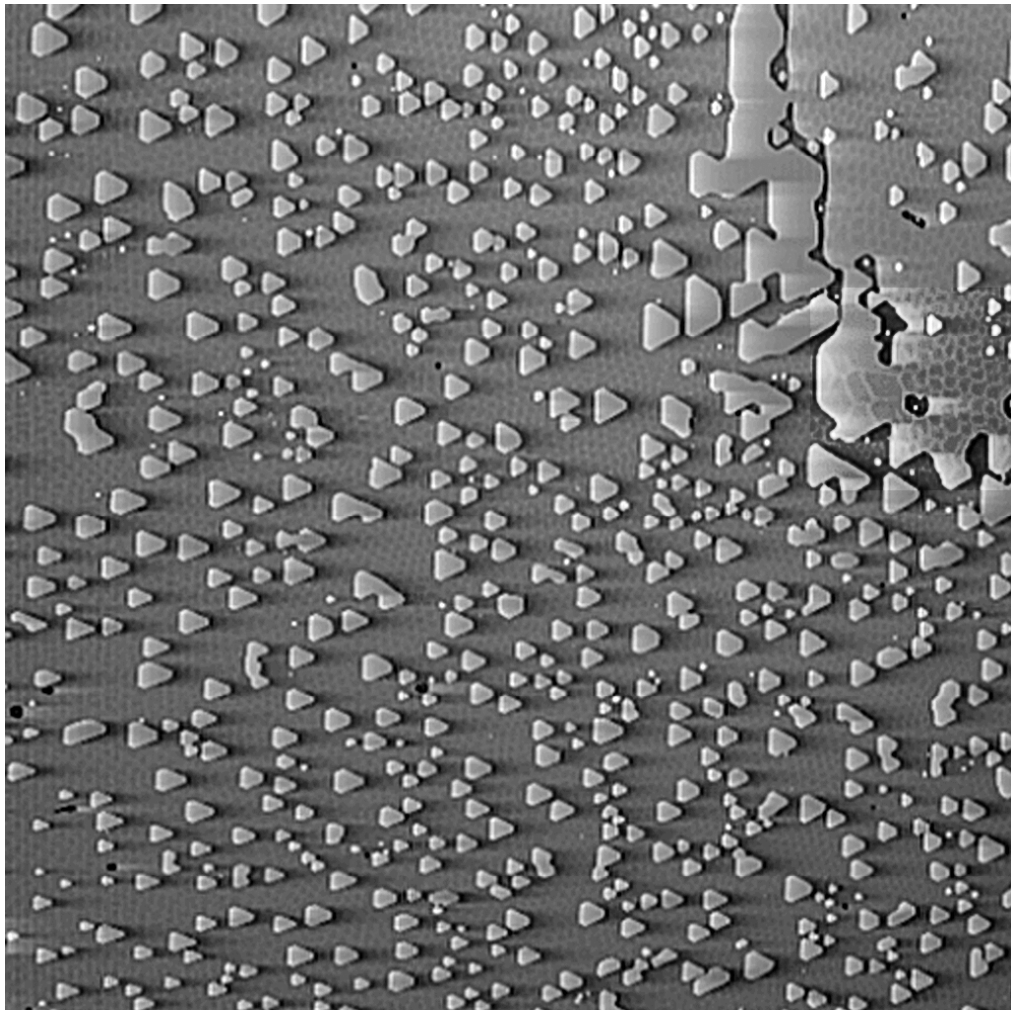

600 K, 5 ML Pt deposited

Fig. 6.10

Strain Relief in Stranski-Krastanov Growth

tetragonal distortion

coherently strained 3D islands

intoduction of misfit dislocation

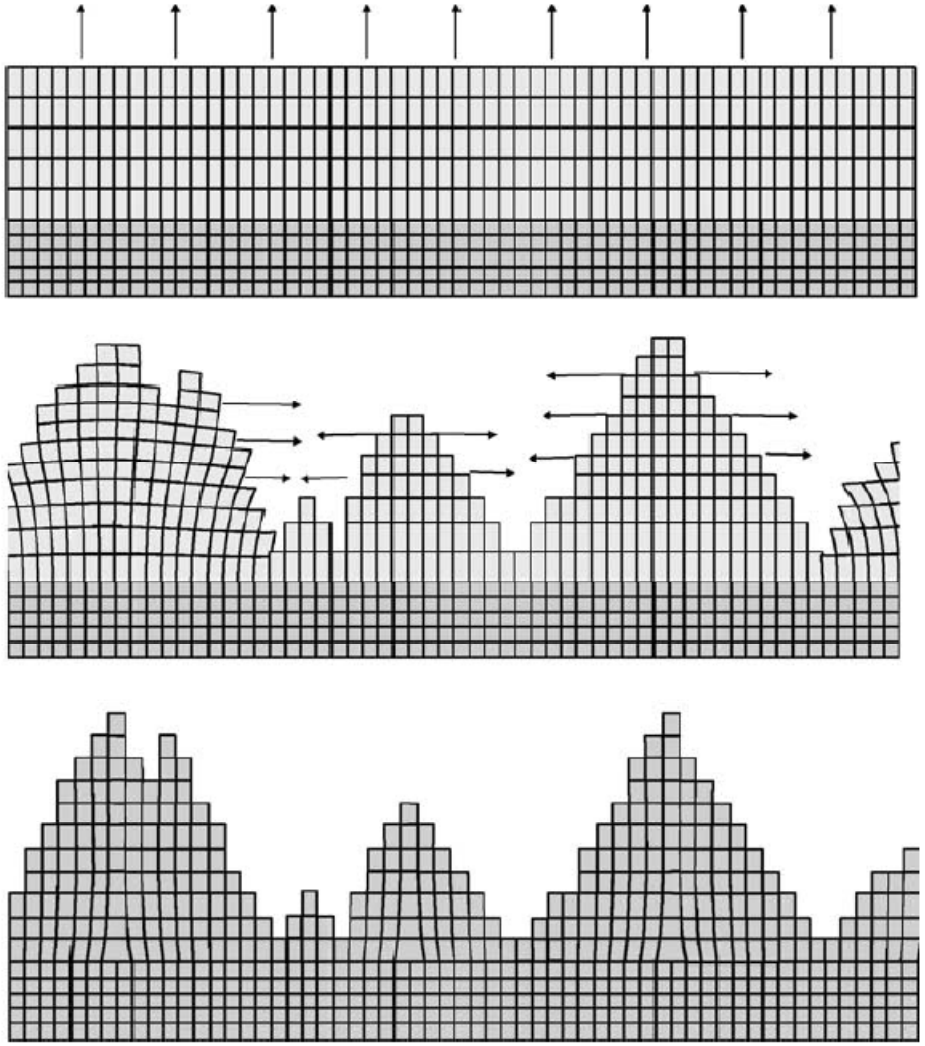

Fig. 6.11

Stranski – Krastanov Growth: Ge Hut-Cluster on Si(001)

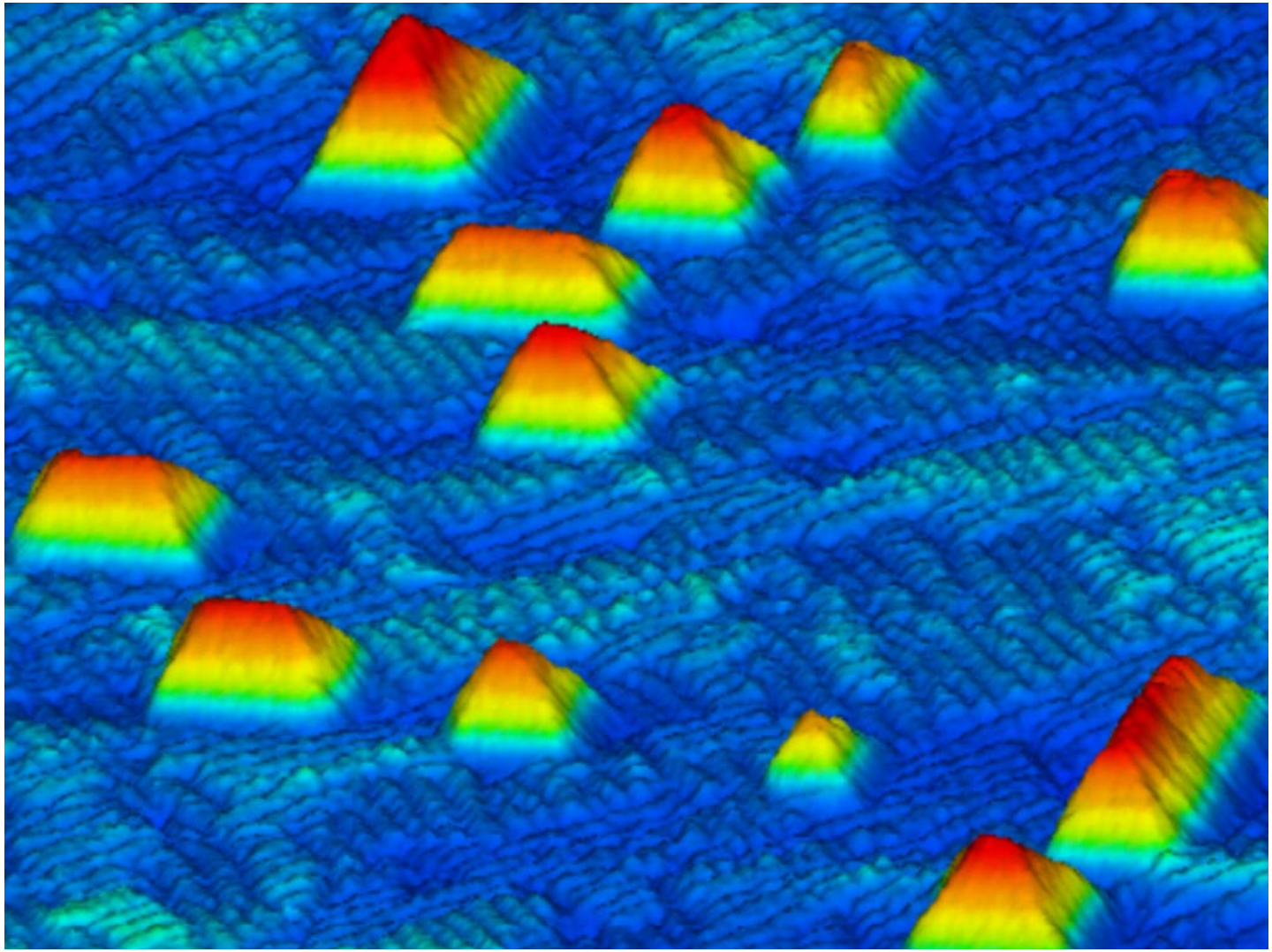

Fig. 6.12

Stages in Si_xGe_{1-x} Epitaxy on Si(001)

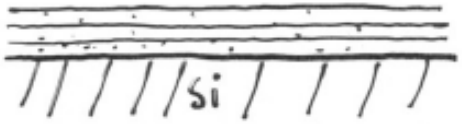

≥ 3 ML Ge, $Si_{1-x}Ge_x$, kohärent

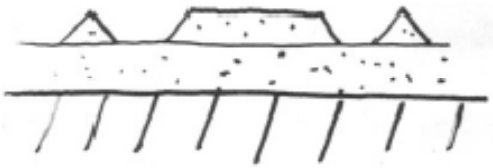

„Hut-Cluster", kohärent
Relaxiation der Spannung

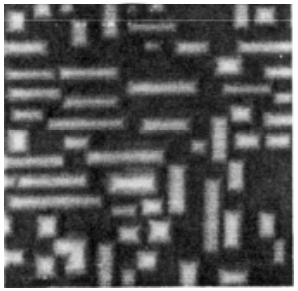

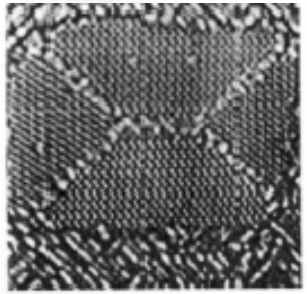

← 400 Å →

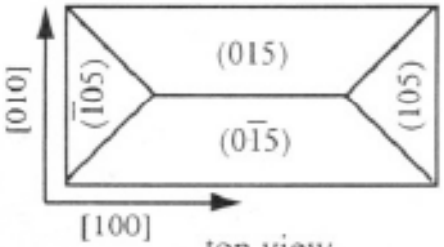

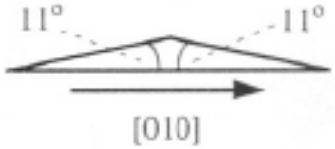

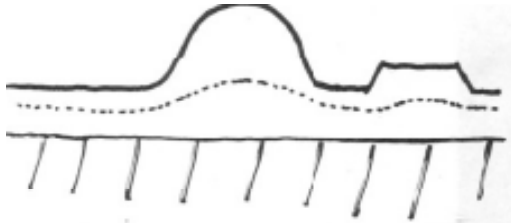

„Dome-Cluster", kohärent
Relaxiation der Spannung

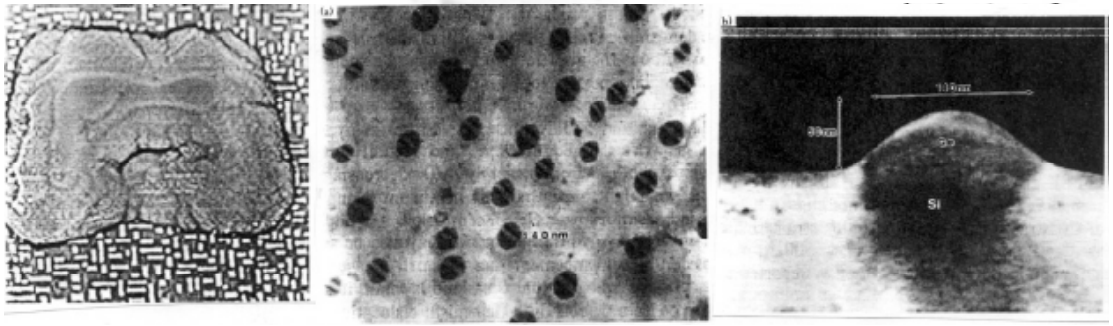

FIG. 4. Plan-view and cross-section TEM images of large coherent SK islands close to their maximum size prior to dislocation introduction. (a) Bright-field image near the [202] Bragg position showing characteristic "bend-contour" contrast due to dome-shaped deformation of the substrate around the island. (b) (400) dark-field image; note strong strain contrast around island.

Fig. 6.13

Stages in Si_xGe_{1-x} Epitaxy on Si(001)

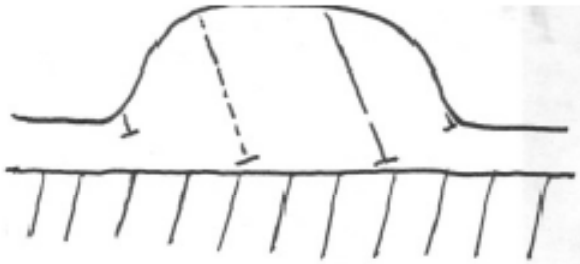

„Dome Cluster", inkohärent Versetzungnukleation

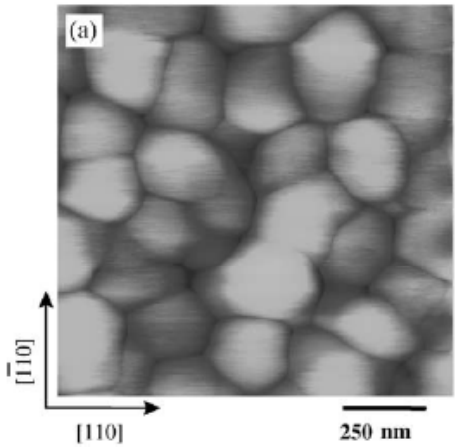

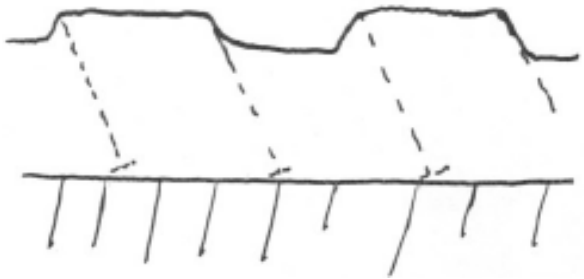

Versetzungsnetzwerk nach Koaleszenz

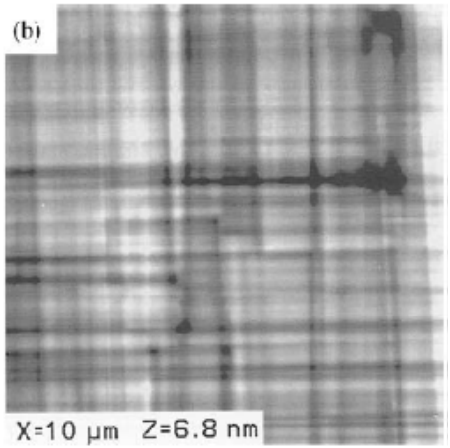

Fig. 6.14

Correlated Nucleation Through Strain

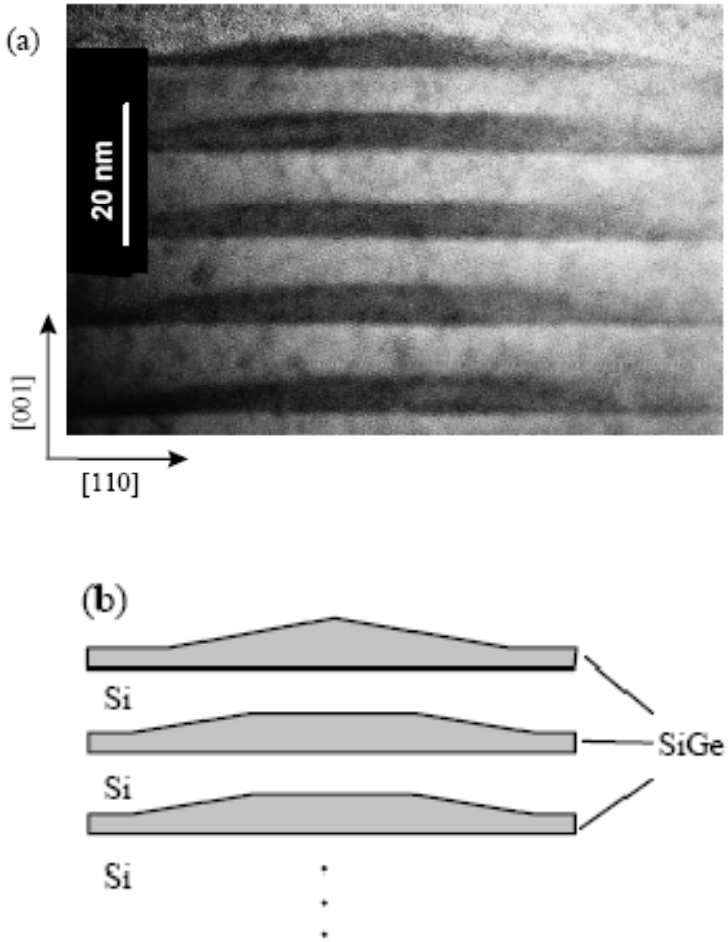

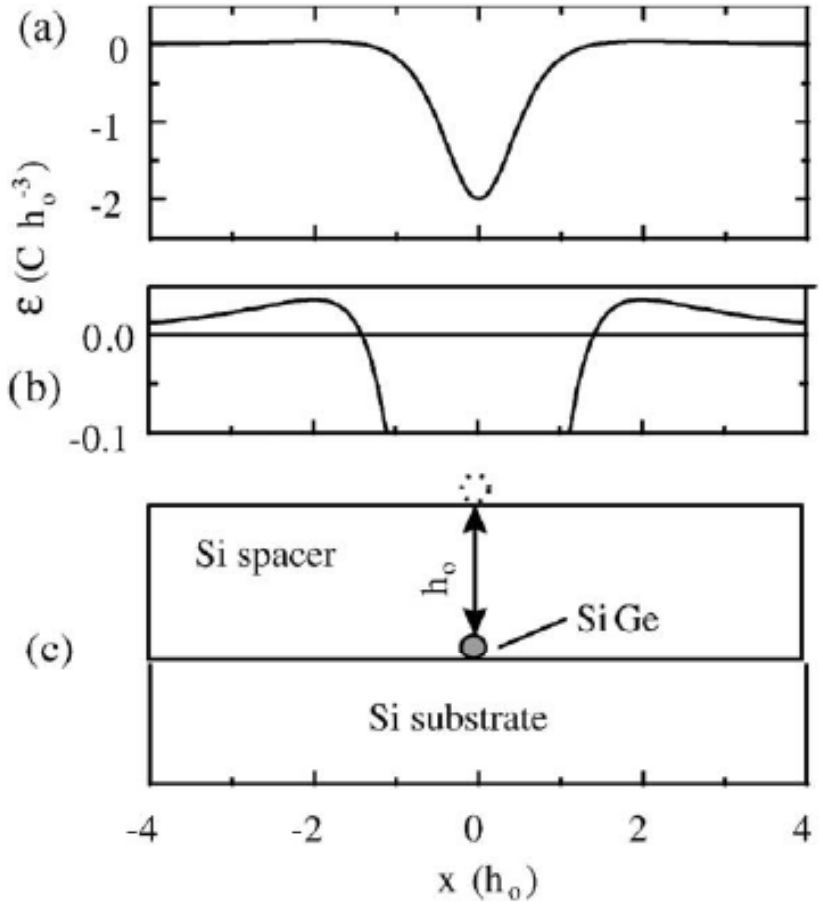

Fig. 6.15

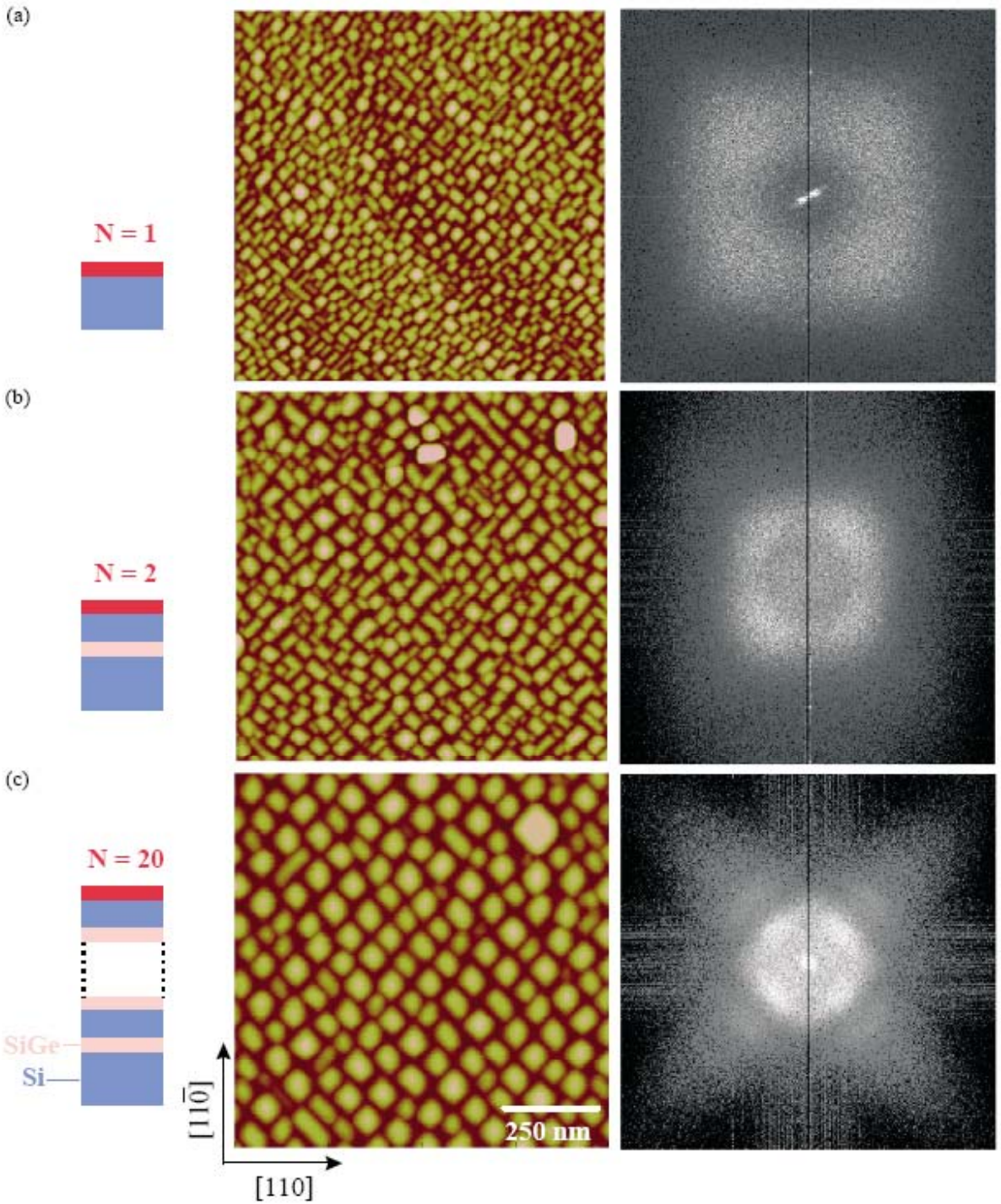

Si/SiGe Multilayer Films

Fig. 6.16

C. Teichert,
Physics Reports 365 (2002) 335

Strain Mechanism for Island Ordering

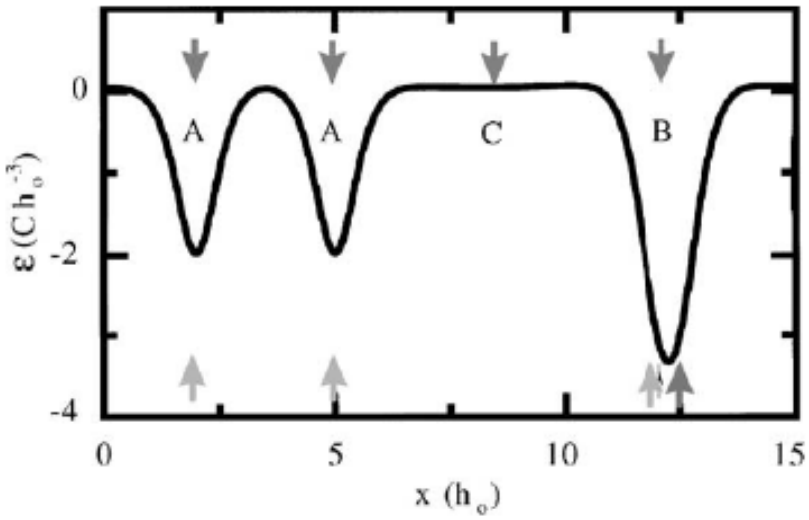

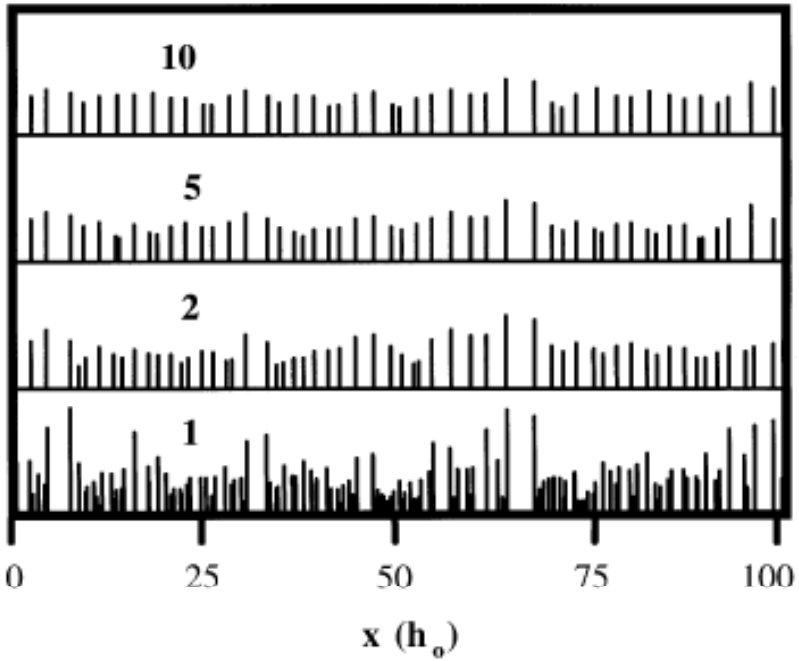

Fig. 53. Surface strain ε versus lateral displacement (in units of the spacer layer thickness h_o) due to four strained islands. Arrows at bottom indicate lateral position of buried islands. Arrows on top indicate minima in ε, i.e., favored positions for subsequent island formation. Properly spaced islands replicate the lateral positions of the underlying ones (labeled A). In addition, there is a "thinning out" of closely spaced islands (B) and possibly a filling in of gaps in the island arrangement (C) (after Tersoff et al. [232]).

Fig. 54. Calculated island positions and sizes in selected successive layers starting from a random arrangement of closely spaced islands. Layer numbers are indicated. Heights of vertical lines represent island volumes, relative to the average for that layer. Only a third of the periodic cell of 300 h_o is shown (from Teichert et al. [223]).

Fig. 6.17

Fcc Quantum Dot Crystals in Strained Layer Epitaxy of $PbSe/Pb_{1-x}Eu_xTe$

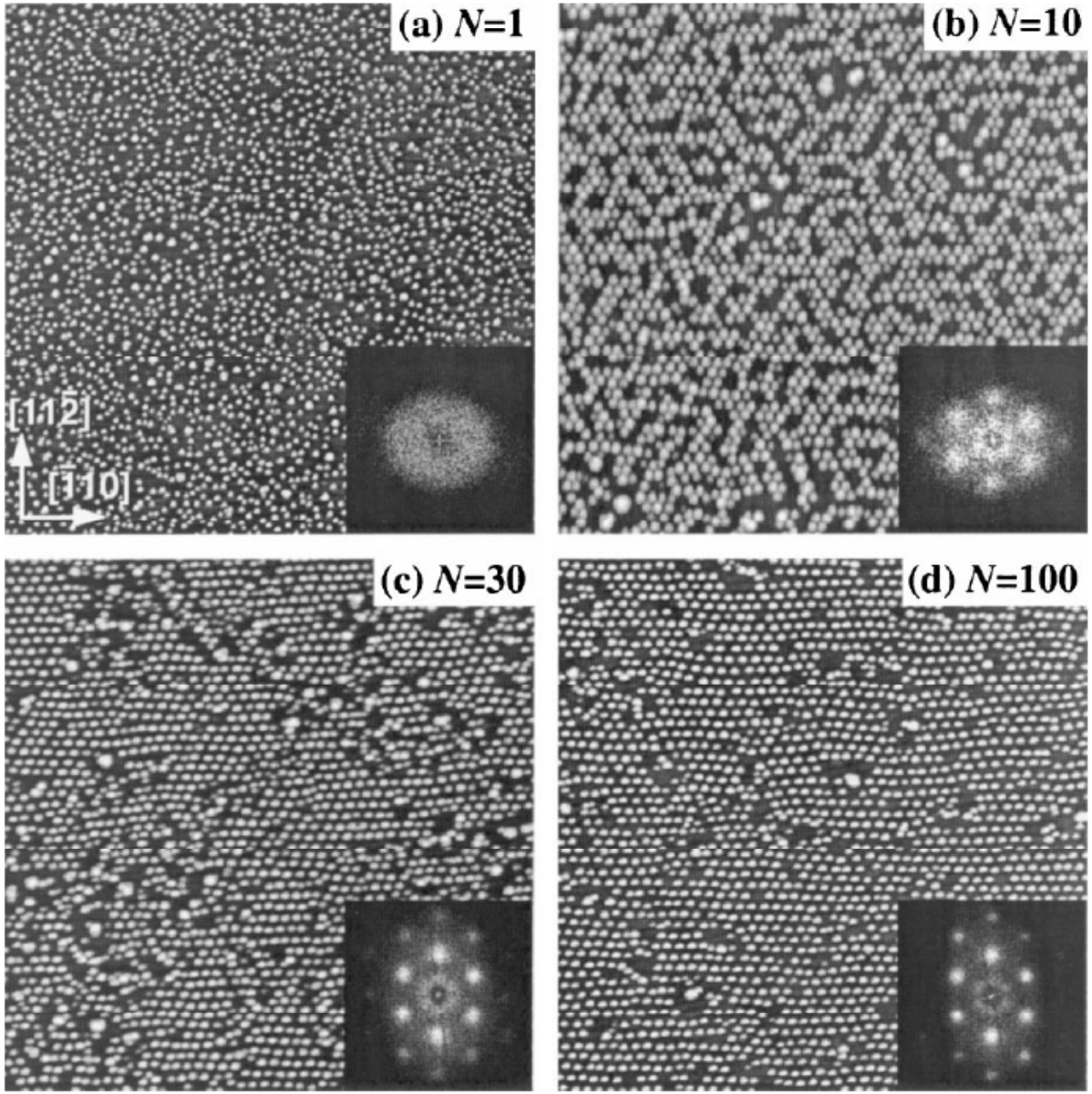

Fig. 6.18

Fcc Quantum Dot Crystals in Strained Layer Epitaxy of $PbSe/Pb_{1-x}Eu_xTe$

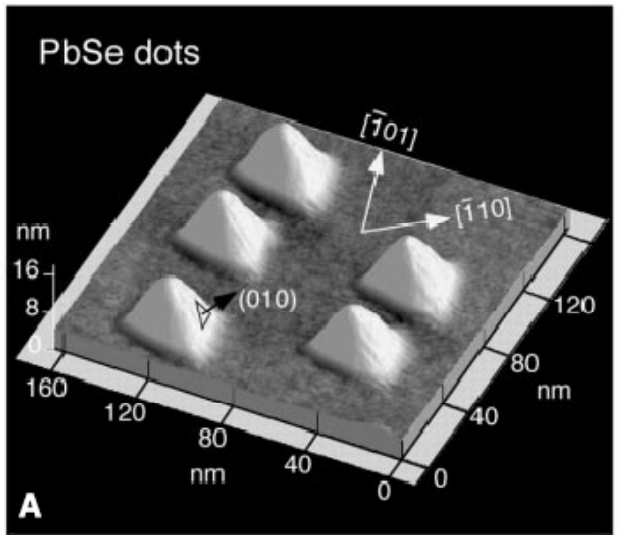

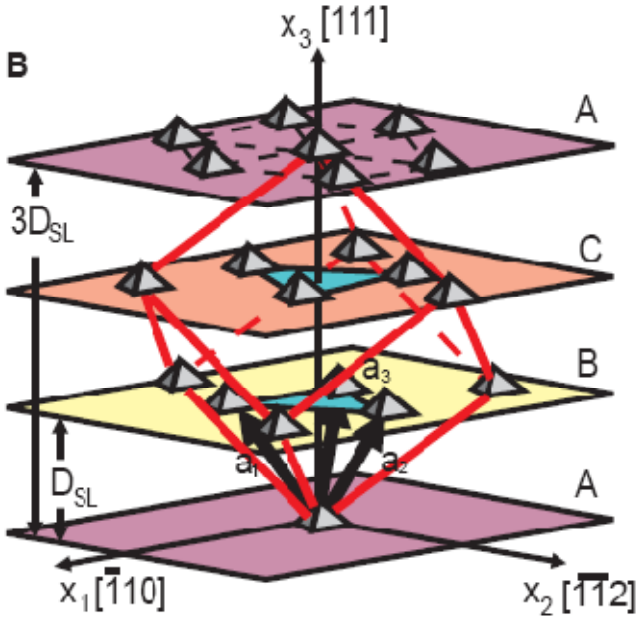

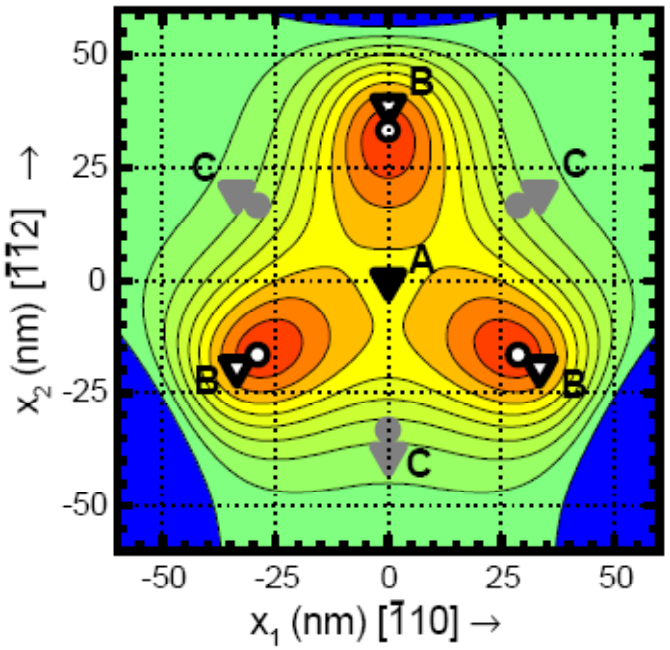

Fig. 4. Distribution of the elastic energy density Σ on the (111) $Pb_{1-x}Eu_xTe$ surface that was calculated for a PbSe force nucleus in the depth of 47 nm. At the minima of Σ (dark orange), the misfit strain is locally reduced by ~2%. The regions with increased Σ are blue. The observed PbSe dot positions at interfaces A, B, and C are denoted by black, gray, and white triangles, respectively. The gray and white circles denote the dot positions in a cubic fcc lattice.

G. Springholz, V. Holy, M. Pinczolits, G. Bauer
Science 282 (1998) 734

Fig. 6.19